Available online at www.sciencedirect.com
SCIENCE DIRECT®
International Journal of Heat and Mass Transfer 48 (2005) 3804–3816
International Journal of HEAT and MASS TRANSFER
www.elsevier.com/locate/ijhmt

Experimental study on condensation heat transfer enhancement and pressure drop penalty factors in four microfin tubes

D. Han [a], Kyu-Jung Lee [b,*]

[a] Institute of Advanced Machinery Design, Korea University, Seoul 136-713, Korea
[b] Department of Mechanical Engineering, Korea University, 5ka-1 Anam-dong, Sungbuk-gu, Seoul 136-713, Korea

Received 2 August 2004; received in revised form 23 November 2004

Abstract

Heat transfer and pressure drop characteristics of four microfin tubes were experimentally investigated for condensation of refrigerants R134a, R22, and R410A in four different test sections. The microfin tubes examined during this study consisted of 8.92, 6.46, 5.1, and 4 mm maximum inside diameter. The effect of mass flux, vapor quality, and refrigerants on condensation was investigated in terms of the heat transfer enhancement factor and the pressure drop penalty factor. The pressure drop penalty factor and the heat transfer enhancement factor showed a similar tendency for each tube at given vapor quality and mass flux. Based on the experimental data and the heat–momentum analogy, correlations for the condensation heat transfer coefficients in an annular flow regime and the frictional pressure drops are proposed.
© 2005 Elsevier Ltd. All rights reserved.

Keywords: Microfin tube; Condensation; Heat transfer; Pressure drop; Correlations

1. Introduction

Since Fujie et al.'s [1] invention, microfin tubes have received a lot of attention because they ensure a large heat transfer enhancement (80–180%) with a relatively small increase in pressure drop (20–80%). Microfin tubes are typically made of copper and have an outside diameter between 4 and 15 mm, have a single set of 50–70 spiral fins with spiral angle between 6° and 30°, and a fin height between 0.1 and 0.25 mm. The heat transfer enhancement is caused by the increase in the surface heat transfer area, the mixing induced by fin in the liquid film, and the surface tension effect on the condensate drainage in microfin tubes.

Numerous researchers [2–10] have proposed condensation heat transfer and pressure drop correlations for microfin tubes. Newell and Shah [11] reviewed the characteristic of two-phase heat transfer, pressure drop, and the effect of void fraction in microfin tubes. García-Valladares [12] reported that additional work was needed to develop a generalized heat transfer correlation for microfin tubes. Wang and Honda [13] evaluated the existing condensation heat transfer correlations for microfin tubes with their collected experimental heat transfer data. They reported that the Yu and Koyama

* Corresponding author. Tel.: +82 23290 3359; fax: +82 2928 9768.
E-mail address: kjlee@korea.ac.kr (K.-J. Lee).

0017-9310/$ - see front matter © 2005 Elsevier Ltd. All rights reserved.
doi:10.1016/j.ijheatmasstransfer.2005.02.041

Nomenclature

A	heat transfer surface area [m^2]
c_p	specific heat of fluid at constant pressure [J/kg K]
D	tube diameter [mm]
dP	pressure drop [N/m^2]
dz	distance along the flow direction [m]
e	fin height [mm]
e^+	roughness Reynolds number [dimensionless] ($=eu_t/v$)
Eh	heat transfer enhancement factor [dimensionless] ($=h_m/h_s$)
f	friction factor [dimensionless]
g	acceleration due to gravity [m^2/s]
G	mass flux [kg/m^2 s]
h	heat transfer coefficients [W/m^2 K]
h_t	heat transfer coefficients in the groove [W/m^2 K]
i	enthalpy [J/kg]
k	thermal conductivity of fluid [W/mK]
L	test section length [m]
m	mass flow rate [kg/s]
n	number of fins [dimensionless]
N	total number of data [dimensionless]
Nu	Nusselt number [dimensionless] ($=hD_i/k$)
p	axial fin pitch [mm] ($=\pi D_i/n\tan\beta$)
PF	pressure drop penalty factor [dimensionless] ($=dP_m/dP_s$)
Pr	Prandtl number [dimensionless] ($=v/\alpha$)
Pr_t	turbulent Prandtl number [dimensionless] ($=\varepsilon_m/\varepsilon_h$)
Q	heat transfer rate [W]
T	temperature [°C]
t_w^+	temperature difference in the groove [dimensionless] ($=\rho c_p u_t/h_t$)
u	fluid time average axial velocity [m/s]
u_t	turbulent friction or shear velocity [m/s] ($=\tau^{0.5}/\rho^{0.5}$)
x	vapor quality [dimensionless]
X_{tt}	Lockhart–Martinelli parameter [dimensionless]
y	distance measured from the duct wall [m]
y^+	wall coordinate [dimensionless] ($=yu_t/v$)

Greek symbols

α	thermal diffusivity [m^2/s]
β	spiral angle [°]
δ	liquid film thickness [m] ($=(1-\lambda)D_i/4$)
Δ	difference [dimensionless]
ε_h	eddy thermal diffusivity for turbulent flow [m^2/s]
ε_m	eddy kinematic viscosity for turbulent flow [m^2/s]
Φ	two-phase frictional multiplier [dimensionless]
λ	void fraction [dimensionless]
v	kinematic fluid viscosity [m^2/s]
θ	apex angle of a fin [°]
ρ	density [kg/m^3]
τ	shear stress [N/m^2] ($=D_i(dP/dz)_{fr}/4$)

Subscripts

exp	experimental
f	refrigerant
fr	frictional
g	gas phase
i	inside
in	inlet
l	liquid phase
lo	liquid only
m	microfin tube
o	outside
out	outlet
pre	pre-heater
pred	predicted value
s	smooth tube
sat	saturation
ts	test section
w	wall or water

[9] correlation gave the best prediction of performance among the empirical correlations. Wang et al. [14] compared the condensation frictional pressure drop correlations for microfin tubes and reported that the Goto et al. [8] correlation showed the best results even though it does not consider any geometrical effects.

The characteristics of smaller diameter tubes must be investigated to develop information for compact size heat exchangers. Although the extensive studies on two-phase heat and flow characteristics in microfin tubes has been done, more research on the characteristics of microfin tubes less than 6 mm in diameter is needed. Although a relatively large number of correlations have been proposed for microfin tubes, the existing correlations need to be evaluated with the experimental data of smaller diameter tubes. Without considering of geometrical effects, heat transfer enhancement cannot be ensured even if smaller size diameter tubes are introduced. Therefore, the heat transfer and frictional pressure drop characteristics of smaller microfin tubes must be

investigated and compared with the smooth tubes. In this study, four different microfin tubes were used with R22, R134a, and R410A. The maximum inside diameters of the tubes were 8.92, 6.46, 5.1, and 4 mm. The effect of the vapor quality and mass flux were investigated in terms of the heat transfer enhancement factor and the pressure drop penalty factor. Finally, a condensation heat transfer correlation and a frictional pressure drop correlation were proposed. Obtained experimental data and other researchers' data were compared with the existing heat transfer and the pressure drop correlations and newly proposed correlations in this study.

2. Experiments

2.1. Experimental apparatus and procedures

Fig. 1 shows the schematic of the experimental apparatus. The system was made up of two independent loops, a low temperature cooling water loop and a high temperature refrigerant loop. The refrigerant loop was composed of a magnetic gear pump, a mass flow meter, a pre-heater, and a heat exchanger. The magnetic gear pump and needle valves controlled the mass flow rate of the refrigerant. The mass flow meter was located between a filter and the pre-heater and measured the mass flow rate of the sub-cooled refrigerant. Its full scale accuracy was ±0.5%. The subcooled refrigerant was heated by the pre-heater to acquire a predetermined inlet vapor quality before entering the test section. Electrically insulated heating wires were wrapped around the surface of copper tubes in the pre-heater. The pre-heater was insulated with glass fibers and rubber. The amount of heat loss from the pre-heater was calibrated through pre-tests with water; this was then correlated to the voltage input. The maximum heat loss in the pre-heater did not exceed 3.2%. The two-phase refrigerant entered the test section and was condensed. Afterwards, the refrigerant was sub-cooled by the additional heat exchanger and went into a liquid receiver. The condensing pressure and temperature of the refrigerants in the system were determined by adjusting the flow rate and the temperature of the water in the heat exchanger. Finally, the sub-cooled refrigerant was re-circulated through the refrigerant loop.

The cooling water loop was composed of a heat exchanger, a volumetric flow meter, and a pump. The cooling water was pumped to the circular-tube annulus, where it absorbed the heat of the condensing refrigerant. The cooling water loop rejected heat to a temperature controlled water bath. The temperature difference between the refrigerant and cooling water (averaged value of inlet and outlet temperatures) was controlled near 15 °C during the experiments. The volumetric flow meter had ±1.5% full scale accuracy. Fig. 2 illustrates the test section. The test section was a horizontal tube-in-tube heat exchanger. The refrigerant flowed through the copper tube and the cooling water flowed through the annulus in the counterflow direction. The effective heat transfer length was 1000 mm. A 19 mm inner diameter acryl tube was used as a circular-tube annulus. A straight tube of 1700 mm in length was placed in front of the test section to stabilize the flow. Because of the thin wall thickness of microfin tubes, it was difficult to make a hole on the surface of microfin tubes for the pressure taps. Therefore, two tees that had a 1.6 mm outside diameter tube were soldered at both ends of each test section. The 1.6 mm outside diameter tubes were connected to a differential pressure transducer. The full scale accuracy of the differential pressure transducer and pressure gauges were ±0.5%. The tee also had a 1.6 mm diameter hole for the insertion of a thermocouple to measure the refrigerant temperature.

In Fig. 2, the lower right side figure illustrates the placement of the refrigerant side measurement instrumentation. The annular side water temperature was measured by four 1.6 mm diameter T-type thermocouples at each inlet and outlet port. Four thermocouples were placed in each location, as shown in Fig. 2 (cross-section B–B). The inlet and outlet water temperatures were determined by an average of the four thermocouples.

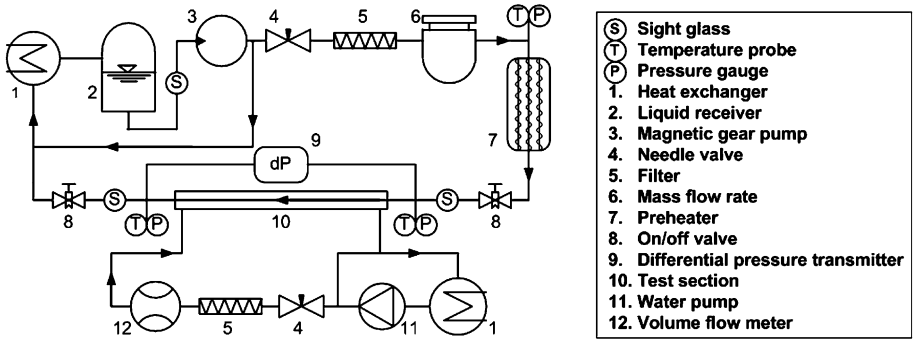

Fig. 1. Schematic diagram of test facility.

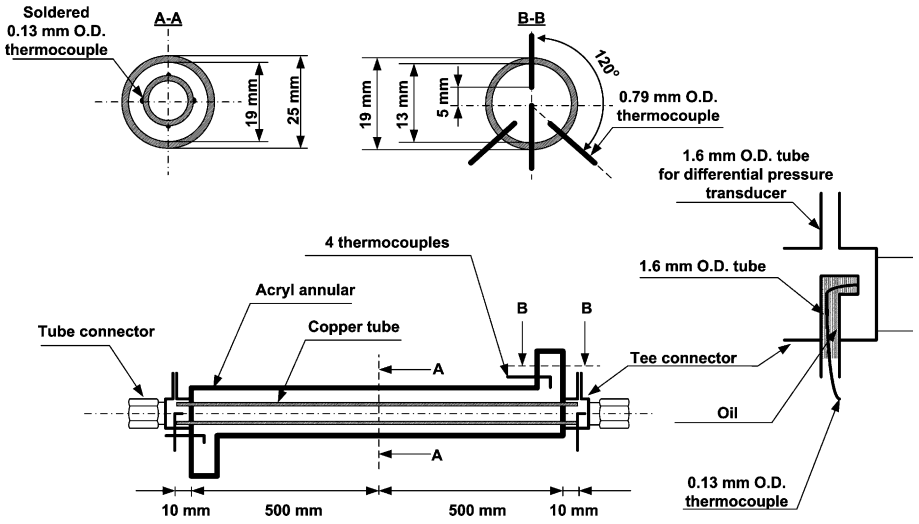

Fig. 2. Schematic diagram of test section.

Four 0.13 mm diameter T-type thermocouples were carefully soldered on top, bottom, right and left sides of copper tube as shown in Fig. 2 (cross-section A–A) to measure the tube wall temperature. The four thermocouples were located in the center of the test section. The test sections were well insulated with the glass fiber and rubber. Through pretest runs, the amount of heat loss was calculated from the energy balances between the inner copper tube side and the annular side. The heat loss was 3% of the total heat transfer rate.

Sight glasses were mounted at the inlet and outlet of the test section to visualize the flow. Steady state was obtained by the control of the inlet temperature and the flow rate of water. All experimental data were recorded under the steady state. Flow condition was considered to be steady state when all temperature oscillations were less than ±0.1 °C.

2.2. Heat transfer data reduction

The subcooled refrigerant enthalpy upstream of pre-heater was determined by measuring its temperature and pressure. Then, the test section inlet enthalpy could be calculated from the heat input of the pre-heater.

$$i_{ts,in} = i_{pre} + Q_{pre}/m_f \tag{1}$$

The condensing heat transfer rates in the test sections were obtained by the mass flow rate and the temperature difference of the cooling water.

$$Q_{ts} = m_w c_{p,w} \Delta T_w \tag{2}$$

The enthalpy of test section outlet was calculated from Eq. (3).

$$i_{ts,out} = i_{ts,in} - Q_{ts}/m_f \tag{3}$$

With the enthalpies calculated, test section inlet vapor quality was given by Eq. (4).

$$x_{ts,in} = (i_{ts,in} - i_l)/i_{lg} \tag{4}$$

The difference of refrigerant vapor quality was determined by Eq. (5).

$$\Delta x = x_{ts,in} - x_{ts,out} = Q_{ts}/m_f \cdot i_{lg} \tag{5}$$

Then, the averaged vapor quality in the test section was found by Eq. (6).

$$x_{ts} = x_{ts,in} - \Delta x/2 \tag{6}$$

Averaged tube outside wall temperature was obtained as follows:

$$T_{w,o} = (T_{w,top} + T_{w,bottom} + T_{w,left} + T_{w,right})/4 \tag{7}$$

The tube inside wall temperature was calculated as follows:

$$T_{w,i} = T_{w,o} + Q_{ts} \ln(D_o/D_i)/2\pi kL \tag{8}$$

Heat transfer coefficients were calculated from the heat transfer rate, the tube inside temperature and the actual tube inside surface area. The actual inside surface areas of microfin tubes were obtained from numerical models.

$$h = Q_{ts}/A(T_f - T_{w,i}) \tag{9}$$

Because of the pressure drop during condensation, the outlet refrigerant temperature of test section was lower than that of inlet. For the 8.92 mm and 6.46 mm ID tubes, the temperature differences were less than 0.2 °C. For the 4 mm ID tube, the maximum temperature drops were 0.5, 2.2, and 0.8 °C for R22, R134a, and R410A, respectively. It assumed that temperature varied linearly in the test section. Therefore, the

averaged values of the inlet and the outlet refrigerant temperatures were used for the calculation of heat transfer coefficients and refrigerants properties.

2.3. Pressure drop data reduction

The two-phase pressure drops are usually composed of a static pressure drop, a momentum pressure drop, a frictional pressure drop, and a port pressure drop. The static pressure drop can be neglected in the horizontal flow. Thus, the frictional pressure drop can be obtained by the elimination of the other pressure drops from the measured pressure drop. The entrance and exit ports pressure drops were evaluated by the loss coefficient concept with equivalent Reynolds number. The loss coefficient was taken from Idelchik [15]. To calculate momentum pressure drops, the void fraction correlation from Yashar [16] for microfin tubes was used. The momentum pressure drop can be expressed as follows:

$$\Delta P_{\mathrm{mom}} = G^2\left[\left\{\frac{(1-x)^2}{\rho_{\mathrm{l}}(1-\lambda)}+\frac{x^2}{\rho_{\mathrm{g}}\lambda}\right\}_{\mathrm{outlet}} - \left\{\frac{(1-x)^2}{\rho_{\mathrm{l}}(1-\lambda)}+\frac{x^2}{\rho_{\mathrm{g}}\lambda}\right\}_{\mathrm{inlet}}\right] \tag{10}$$

where, the void fraction, λ is

$$\lambda = \left[1+\left(\frac{1-x}{x}\right)\left(\frac{\rho_{\mathrm{g}}}{\rho_{\mathrm{l}}}\right) \times\left\{1+1.3Re_{\mathrm{lo}}^{-0.19}\left(\frac{\rho_{\mathrm{l}}}{\rho_{\mathrm{g}}}\right)^{0.72}\left(\frac{x}{1-x}\right)^{0.5}\right\}\right]^{-1} \tag{11}$$

2.4. Uncertainties

The maximum uncertainties are ±2.6% for the water temperature difference, ±2.2% for the temperature difference between tube wall and refrigerant, ±2.8% for the mass flow rate of water, ±2.4% for the mass flux of refrigerant, ±3.4% for the heat flux of test section, ±4.3% for the vapor quality, ±9.7% for the pressure drop, and ±11.1% for the local Nusselt number. The largest uncertainties occurred in the low mass flux region. The uncertainties of the Nusselt number varied from ±7.3% to ±11.1%. The procedures of ASME standard [17] were used for the calculation of all uncertainties. All the uncertainties were calculated at the 95% confidence level.

2.5. Tube geometries and test conditions

Table 1 shows the specifications of microfin tubes and working conditions. Fig. 3 shows the typical geometry of microfin tubes. The principal geometrical param-

Table 1
Geometries of test tubes and working condition

D_{i} [mm]	e/D_{i}	β [°]	θ [°]	n	$A_{\mathrm{m}}/A_{\mathrm{s}}$	G [kg/m^2 s]	T_{c} [°C]	Refrigerant
4	0.0325	9	40	60	1.895	456–1110	18.5–33.8	R134a, R22, R410A
5.1	0.0255	10.3	40	60	1.705	287–921	19.1–32.2	
6.46	0.0232	18	53	60	1.616	178–521	19.0–31.7	
8.92	0.0135	25	48	60	1.446	91–404	20.1–32.0	

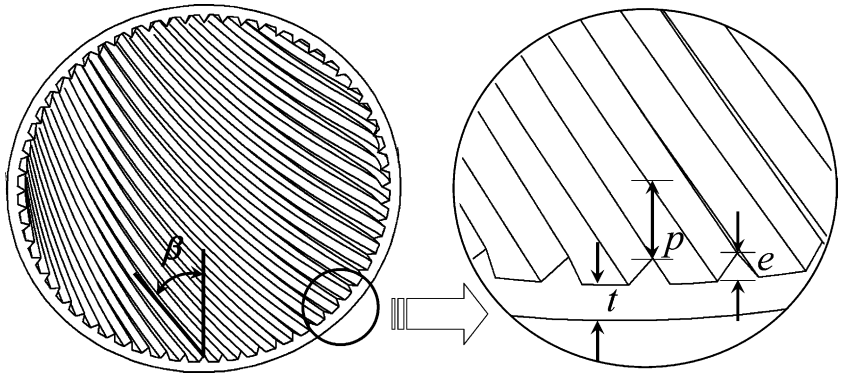

Fig. 3. Typical geometry of microfin tubes.

eters of microfin tubes are the fin height (e), the spiral angle of fins (β), the axial fin pitch (p), the number of fins (n), and the apex angle of a fin (θ). Four different microfin tubes were tested. The maximum inside diameters of tubes were 8.92, 6.46, 5.1, and 4 mm. Other geometrical factors like the spiral angle, the relative roughness (fin height) and the apex angle varied from one another. The surface area enhancement ratio of each tube was calculated with the same ID smooth tube. A 7.92 mm inside diameter smooth tube was also tested to verify the experimental apparatus. R22, R134a, and R410A were used as the working fluids for all the tubes. Mass flux and condensation temperature are also shown in Table 1.

3. Results

3.1. Flow regime

Several researchers have tried to visualize the flow pattern in microfin tubes to investigate the flow mechanism. Among them, Censi et al. [18] proposed a relatively simple flow pattern map with R134a and a single microfin tube. Although Censi et al.'s [18] flow pattern map was developed with limited data, it is useful for flow pattern prediction.

Fig. 4 shows the flow pattern in terms of modified fluid velocity and the Lockhart–Martinelli parameter. As condensation proceeds, all test runs start from the left side of the graph and move to the right. With the increase of the mass flux and vapor quality, the flow pattern moved to the annular flow regime. 38% of the experimental data of the 8.92 mm inside diameter tube were located in the stratified wavy flow regime. Most experimental data of 6.46, 5.1, and 4 mm inside diameter tube were placed in the annular flow regime.

Censi et al. [18] detected an earlier transition into the annular flow regime in their microfin tube. Surface tension and the fin spiral angle may help to change the stratified wavy flow into the annular flow. Oh and Bergles [19] also visualized the flow pattern in microfin tubes and reported that a microfin tube with 6° spiral angle groove was the most effective in pulling the liquid upward at 200 kg/m^2 s and a tube with 18° spiral angle groove was the most efficient in uniform liquid distribution at 50 kg/m^2 s. This means that flow pattern depends on the geometry of tube. Therefore, additional works are needed to develop the flow pattern map and investigate the flow mechanism in microfin tubes.

3.2. Smooth tube

To verify the experimental apparatus and data, a 7.92 mm inside diameter smooth tube was tested and its heat transfer coefficients and pressure drops were compared with existing smooth tube correlations. The mass flux range for the smooth tube was 80–450 kg/m^2 s. Condensation temperature and vapor quality ranges were similar to those of the microfin tubes. R22, R134a, and R410A were also used as working fluids for the smooth tube. Cavallini et al. [20] recommended the Kosky and Staub [21] condensation heat transfer correlation in the annular flow regime and the Jaster and Kosky [22] correlation in the stratified flow regime. After the application of both correlations, the higher of the two values is taken as the predicted heat transfer coefficient. Ould et al. [23] reported that the Müller-Steinhagen and Heck [24] frictional pressure drop correlation produced the best result for smooth tubes. Figs. 5 and 6 show the comparison between experimental data and predicted values of the correlations for the pressure drops and the heat transfer coefficients of the smooth tube. The Müller-Steinhagen and Heck [24] frictional pressure drop correlation slightly over-predicted for R410A and under-predicted for R22. Ninety

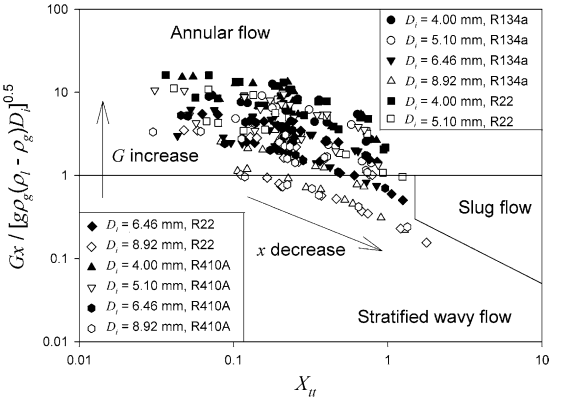

Fig. 4. Flow regime map on the Censi et al. [18] map.

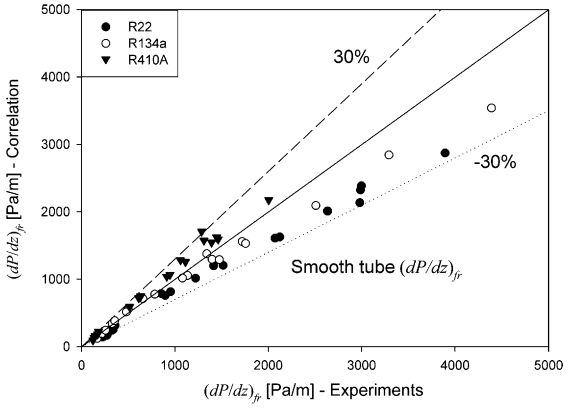

Fig. 5. Experimental smooth tube pressure drop data versus the existing correlation.

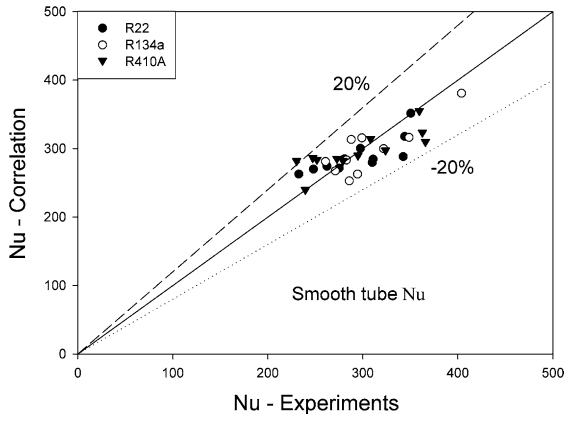

Fig. 6. Experimental smooth tube Nusselt number versus the existing correlations.

three percentage of the frictional pressure drop data were placed within ±30% deviation and 97% of the Nusselt number data were placed within ±20% deviation.

3.3. Pressure drop penalty factor

Frictional pressure drop characteristics of microfin tubes were investigated in terms of the pressure drop penalty factor (*PF*). The *PF* is the ratio of frictional pressure drop per unit length of a microfin tube and that of a smooth tube at the same maximum inside diameter and operating condition. The Müller-Steinhagen and Heck [24] frictional pressure drop correlation was used to evaluate the corresponding smooth tube pressure drop.

Figs. 7 and 8 show the effect of vapor quality and mass flux on the PF_{local}, respectively. The PF_{local} in Fig. 7 is the local value at specific mass flux, vapor quality, and condensation temperature. Peak points were detected and those points varied as tube geometry and mass flux changed. The PF_{local} increased with vapor quality in the lower vapor quality region and decreased after reaching the upper limit of 0.6. This phenomenon can be explained by turbulence generation from the microfins. With vapor quality increasing, microfins extrude over the liquid film. These extruded microfins slightly increase the frictional loss in the medium vapor region (0.4–0.6 vapor quality). But in the high vapor quality region, the turbulence level is high enough that contribution to turbulence generation by extruded microfins decreases with the vapor quality. Eckels and Tesene [25] reported that pressure drop penalty factors generally decreased with vapor quality at 250 kg/m^2 s in an 8.92 mm inside diameter tube for R22, R410A, R407C, and R134a. However, they evaluated *PF* values with an 8.01 mm inside diameter smooth tube at the same mass flux and vapor quality. Therefore, their comparison might have inaccurate information. Cavallini et al.'s [26] R134a experimental data at 200 kg/m^2 s in a 7.69 mm inside diameter tube also had a peak point like this experiment. However, their peak point was placed in the lower quality region (0.3–0.4 vapor quality). This may be an effect of the fin height difference. Cavallini's microfin tube had a 0.23 mm fin height. Higher fins may extrude over the liquid film at the lower vapor quality region. These differences between experimental results may also come from the flow regime and the tube geometries. Therefore, flow patterns with

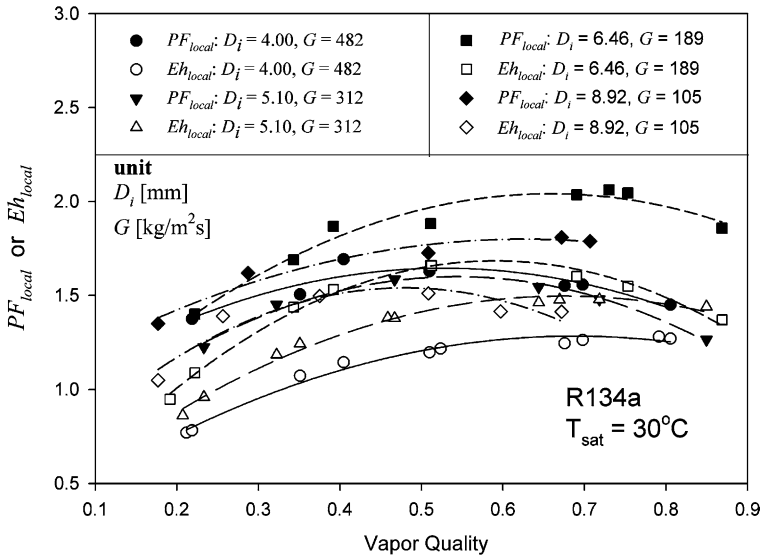

Fig. 7. PF_{local} and Eh_{local} versus vapor quality.

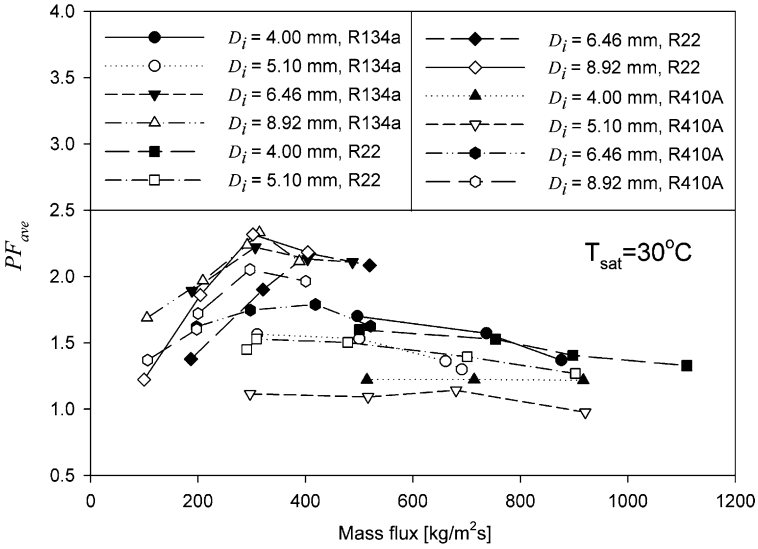

Fig. 8. PF_{ave} versus mass flux.

consideration for the tube geometries should be investigated to predict accurate two-phase characteristics in microfin tubes.

The effect of refrigerants and mass flux on pressure drop penalty factor is shown in Fig. 8. The values of the PF_{ave} shown in Fig. 8 were averaged over vapor quality at a specific mass flux and condensation temperature. Therefore, the values of the PF_{ave} in Fig. 8 were defined as follows:

$$PF_{ave} = \frac{\sum PF_{local} x_{local}}{\sum x_{local}} \quad (12)$$

Regardless of refrigerant, each tube shows a similar tendency for mass flux variation. The 8.92 and the 6.46 mm inside diameter tubes had peak points. Flow regime transition might be one of the reasons for this phenomenon. Censi et al. [18] observed the flow pattern of a 7.69 mm inside diameter microfin tube with R134a and reported that the stratified wavy flow pattern was changed into annular flow at about 200 kg/m^2 s and 0.5 vapor quality. The 5.1 and the 4 mm inside diameter tubes showed decreasing tendencies with a relatively gentle slope. The working condition of the 5.1 and the 4 mm inside diameter tubes were placed in a higher mass flux region. Therefore, the flow regime of the 5.1 and the 4 mm inside diameter tubes remained annular without the flow pattern transition as shown in Fig. 4. Another interesting point is that R410A has the lowest pressure drop penalty factor. This is because of the Müller-Steinhagen and Heck [24] correlation's slight (about 20%) over-predicting tendency for R410A. Moreover, for R22 and R134a, the Müller-Steinhagen and Heck [24] correlation showed a slightly under-predicting tendency. Therefore, the pressure drop penalty factor does not seem to have a significant difference among the tested refrigerants. The Müller-Steinhagen and Heck [24] correlation's over-predicting tendency for R410A may explain the lower PF_{ave} of the 4 and the 5.1 mm ID microfin tubes. Hence, it is needed to obtain experimental data with the same ID smooth tube or develop an accurate correlation in order to understand the characteristic of smaller diameter microfin tubes.

3.4. Heat transfer enhancement factor

The heat transfer characteristics of microfin tubes were investigated in terms of the heat transfer enhancement factor (Eh). The Eh was defined as the ratio between heat transfer coefficient for a microfin and that of a smooth tube at the same operating condition and maximum inside diameter. ($Eh = h_m/h_s$) Kosky and Staub [21] condensation heat transfer correlation and Jaster and Kosky [22] correlation were used to evaluate the smooth tube Nusselt number with the same inside diameter tube at the identical working conditions (vapor quality, mass flux, and saturation temperature).

Fig. 7 also shows Eh_{local} values with vapor quality. Fig. 9 shows the effect of mass flux on the Eh_{ave}. The Eh_{local} and the Eh_{ave} were defined in the same manner as the PF_{local} and the PF_{ave}. The area of microfins in vapor increases as vapor quality increases. Exposed microfins in direct contact with the vapor phase help to increase the heat transfer. Moreover, the decrease of the liquid film with vapor quality increasing promotes the surface drainage between microfins. In the higher vapor velocity region, turbulence by fluid velocity is strong enough that the effect of the fins may be lessened. Because the increase of mass flux promotes flooding of

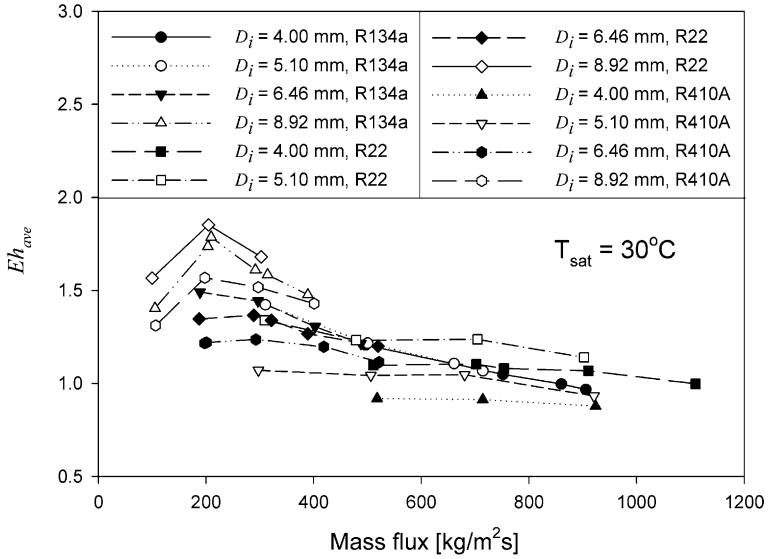

Fig. 9. Eh_{ave} versus mass flux.

liquid over the grooves and this phenomenon reduces the fin effect, the contribution of fins on the heat transfer enhancement is reduced and the heat transfer surface area augmentation becomes the dominant factor for the heat transfer enhancement in microfin tubes in the very high mass flux region ($G \geqslant 400$ kg/m^2 s).

Eckels and Tesene [27] tested an 8.92 mm inside diameter microfin tube with R22, R410A, R134a, and R407C. They reported that the Eh_{local} decreased with vapor quality at a higher mass flux (600 kg/m^2 s) but the Eh_{local} had concave point at a lower mass flux (250 kg/m^2 s). This occurred for all of the tested refrigerants except R134a. They evaluated the Eh_{local} with a different inside diameter smooth tube like their PF values. Therefore, their results may be different if they evaluate the Eh_{local} with the use of the identical inside diameter smooth tube. Cavallini et al. [28] reported that the tendency of the Eh_{local} with vapor quality and mass flux. In the lower mass flux region, Eh_{local} increased with vapor quality. In the higher mass flux region, vapor quality did not make any significant difference on the Eh_{local}. They also reported that heat transfer enhancement factor had a peak point like this study. Censi et al. [18] also reported similar results like this study.

Another interesting point is that the Eh_{ave} were lower than unity at the higher mass flux region. However, heat transfer coefficients of microfin tubes are larger than those of smooth tubes if the heat transfer area augmentation is considered. Similar results were also reported by Censi et al. [18]. This implies that the effect of microfins is reduced at the higher mass flux region. Therefore, microfin tubes may be more effective in the lower mass flux region.

The effect of vapor quality and mass flux were quite similar to those of the pressure drop penalty factor. This implies that heat transfer mechanism is closely related to pressure drop in the tested microfin tubes like heat–momentum analogy in the single-phase.

The heat transfer enhancement factor was different for each refrigerant. The heat transfer enhancement value of R410A was the lowest among the tested refrigerants. This phenomenon may be explained with the prediction accuracy of the smooth tube correlation (±20%) and the experimental uncertainties (±11%). On the other hand, Jung et al. [29] explained this difference in other way. Their Eh_{ave} of R22 was 0.25–0.5 higher than that of R410A. Furthermore, their maximum Eh_{ave} difference between R407C and R22 was 0.73. They reported that their tested tube (8.92 mm ID, 0.2 mm fin height, 18° helix angle, 60 fins) might be optimized for R22 and new tube geometries must be suggested for R410A and R407C, separately. This means that each refrigerant may have a specific optimized geometry to obtain the maximum heat transfer enhancement. To evaluate their statement, additional accurate experimental verifications with various tubes and refrigerants are needed.

3.5. Correlations

Based on the experimental data, a relatively simple condensation frictional pressure drop correlation for the four microfin tubes was developed with the two-phase frictional parameter, Φ_l. The frictional pressure gradient for the two-phase flow was related to the pressure gradient for liquid phase by

$$\left(\frac{dP}{dz}\right)_{fr} = \Phi_l^2 \frac{f_l[G(1-x)]^2}{2D_i\rho_l} \tag{13}$$

where, f_l and Φ_l can be obtained from Eqs. (14) and (15), respectively.

$$f_l = 0.193\left[\frac{G(1-x)D_i}{\mu_l}\right]^{-0.024}\left(\frac{p}{e}\right)^{-0.539} \quad (14)$$

$$\Phi_l^2 = 2.684X_{tt}^{-1.946} \quad (15)$$

where, X_{tt} is the Lockhart–Martinelli parameter.

Table 2 shows the root mean square (r.m.s.) deviation (%) of existing correlations and the proposed correlation of this study. This r.m.s. term is defined as follows.

$$\text{r.m.s.} = \sqrt{\frac{1}{N}\sum\left(\frac{\text{data}_{pred} - \text{data}_{exp}}{\text{data}_{exp}}\right)^2} \quad (16)$$

Although the Newell and Shah [5] correlation does not consider any geometrical effect, their correlation showed the best overall predicting result for this study. The best predicting correlation was different for each tube type and refrigerant. The Goto et al. (2) [8], the Newell and Shah [5], and Eqs. (13)–(15) gave the best results for R134a, R22, and R410A, respectively (the Goto et al. [8] (1) and (2) denotes the vapor and liquid phase correlations, respectively). Newell and Shah [5] predicted the best for 4 and 5.1 mm inside diameter tubes. Choi et al. [7] and the Goto et al. (1) [8] showed the best predicting performances for 6.46 and 8.92 mm inside diameter tubes, respectively.

A heat transfer correlation was developed for the annular flow regime in this study. It is assumed that liquid film thickness is uniform around the tube periphery because of the greater influence of shear force. Since the vapor core is very turbulent, radial temperature gradients and the temperature in the vapor core are neglected. Temperatures in the vapor core and at the liquid–vapor interface are assumed to be equal to the saturation temperature. From the relationship between heat flux and temperature distribution, following integral form can be expressed as

$$\int_0^T dT = \frac{Q}{\rho c_p A}\int_0^\delta \frac{dy}{\alpha + \varepsilon_h} \quad (17)$$

Through the introduction of the non-dimensional distance from the wall in wall coordinates, $y^+(=yu_t/v)$, Eq. (17) can be written in two parts corresponding to the semi-stagnant fluid and the fully turbulent region at the fin tip. Eq. (17) can be written as

$$\frac{\rho c_p u_t}{h} = \int_0^{\delta^+}\frac{dy^+}{1/Pr + \varepsilon_h/v} = t_w^+ + \int_{e^+}^{\delta^+}\frac{dy^+}{1/Pr + \varepsilon_h/v} \quad (18)$$

where, u_t is the turbulent frictional velocity

$$u_t = \left(\frac{\tau}{\rho}\right)^{0.5} = \left\{\frac{D_i}{4\rho}\left(\frac{dP}{dz}\right)_{fr}\right\}^{0.5} \quad (19)$$

In Eq. (18), $1/Pr$ can be neglected in the fully turbulent region. t_w^+ $(=\rho c_p u_t/h_t)$ represents the temperature difference (non-dimensional) in the groove and contains the local heat transfer coefficient in the groove, h_t.

Generally, roughness Reynolds number at the fin tip in the annular flow regime exceeded 21 in this experiment. According to Wang et al. [30], fully turbulent flows in microfin tubes were achieved at the roughness Reynolds number of 23. This means that most of the liquid film above the fin tip is fully turbulent flow in the annular flow regime. For the fully turbulent region, shear stress can be expressed as

$$\frac{\tau}{\rho} = \varepsilon_m\frac{\partial u}{\partial y} \quad (20)$$

Hence, ε_h can be expressed using turbulent Prandtl number and shear stress terms. Because the liquid layer is very thin, shear stress can be assumed as constant in

Table 2
r.m.s. deviation for pressure drop

Refrigerant	D_i [mm]	Choi et al.	Nozu et al.	Haraguchi et al.	Kedzierski and Goncalves	Cavallni et al.	Goto et al. (1)	Goto et al. (2)	Newell and Shah	This work
R134a	4	47.2	148.9	113.4	56.9	13.2	10.6	16.6	21.9	32.7
	5.1	36.0	104.1	79.0	34.3	13.7	11.6	22.8	19.6	35.2
	6.46	13.4	26.1	12.5	15.9	23.2	27.5	22.8	40.5	36.7
	8.92	17.6	15.1	22.9	31.6	22.8	28.5	21.8	38.2	45.2
R22	4	48.0	172.7	132.0	58.9	25.8	22.2	33.3	24.7	27.6
	5.1	40.9	126.0	96.8	39.9	27.5	24.1	33.6	20.1	29.2
	6.46	69.2	105.8	76.0	65.3	63.1	53.8	57.9	47.4	50.3
	8.92	36.2	30.8	13.3	35.3	40.4	23.2	26.6	35.5	30.2
R410A	4	73.9	269.6	195.9	89.9	56.7	57.7	84.1	9.9	23.8
	5.1	72.6	211.4	158.0	73.0	59.9	66.9	89.2	14.7	27.4
	6.46	14.2	77.0	35.5	13.2	12.4	14.1	24.7	34.3	15.7
	8.92	18.6	33.7	18.8	33.2	19.5	17.0	22.5	40.5	30.8
Total		45.3	130.8	96.9	49.9	36.4	34.8	44.6	32.0	33.7

the liquid layer and the universal velocity distribution can be applied in the turbulent region, Eq. (18) can then be reformed as follows;

$$\frac{\rho c_p u_t}{h} = t_w^+ + \int_{e^+}^{\delta^+} \frac{2.5 Pr_t \, dy^+}{y^+} \tag{21}$$

t_w^+ was correlated with e^+ ($=eu_t/v$) and Pr.

$$t_w^+ = 0.904 e^{+0.592} Pr^{0.729} \tag{22}$$

The turbulent Prandtl number was assumed as 0.85.

The final form of heat transfer coefficient correlation is

$$h = \frac{\rho c_p u_t}{0.904 e^{+0.592} Pr^{0.729} + 2.1335 \ln(\delta/e)} \tag{23}$$

where, liquid film thickness ($\delta = (1-\lambda)D_i/4$) was obtained from Yashar's [16] void fraction correlation. When liquid film thickness is less than a fin height, the logarithm term of Eq. (23) is neglected. This correlation can be applied in the annular flow regime. The annular flow regime can be discerned using the Censi et al. [18] flow regime map.

Table 3 shows the root mean square (r.m.s.) deviation (%) for condensation heat transfer coefficients. The Yu and Koyama [9] correlation gave the best prediction for R134a while Eq. (23) showed the best results for the R22 and R410A data. Eq. (23) also gave the best results for the 4 and the 5.1 mm inside diameter tube. For the 6.46 and the 8.92 mm inside diameter tube, the Kedzierski and Goncalves [4] and the Yu and Koyama [9] correlations produced the best predicting performances, respectively. The overall r.m.s. deviation of Eq. (23) was the lowest among correlations for this experimental data. These proposed correlations for the frictional pressure drops and the condensation heat transfer coefficients were also compared to the open experimental data (518 data for the pressure drop and 1593 data for the heat transfer coefficient) of NIST reports [31,32]. Their pressure drop data were composed of three different tubes (8.92, 7.33, 14.68 mm ID tubes) with seven refrigerants (R134a, R22, R410A, R502,

Table 3
r.m.s. deviation for heat transfer coefficients

Refrigerant	D_i [mm]	Cavallini et al.	Yu and Koyama	Kedzierski and Goncalves	Shikazono et al.	This work
R134a	4.0	52.8	19.2	10.2	39.8	33.6
	5.1	58.4	14.9	22.4	61.8	38.9
	6.46	48.3	8.8	17.6	63.8	25.8
	8.92	47.9	27.7	38.8	73.4	24.4
R22	4.0	20.3	73.6	43.4	23.0	11.9
	5.1	37.1	13.4	11.6	54.5	25.2
	6.46	22.8	15.0	5.7	61.0	9.9
	8.92	34.7	23.8	36.3	64.8	24.8
R410A	4.0	16.2	97.8	53.9	14.0	19.0
	5.1	18.6	61.5	28.1	29.9	18.7
	6.46	14.6	20.6	11.4	49.3	12.5
	8.92	12.9	7.3	24.2	55.3	10.6
Total		35.8	42.3	29.8	53.7	22.6

Table 4
r.m.s. deviation for NIST data

Pressure drop	NIST	This work	Total	Heat transfer coefficients	NIST	This work	Total
Choi et al.	24.4	45.3	36.4	Cavallini et al.	36.6	35.8	36.5
Nozu et al.	54.2	130.8	43.9	Yu and Koyama	69.2	42.3	66.1
Haraguchi et al.	25.8	96.9	61.8	Kedzierski and Goncalves	23.0	29.8	24.1
Kedzierski and Goncalves	27.0	49.9	40.1	Shikazono et al.	34.2	53.7	37.6
Cavallni et al.	23.5	36.4	32.2	This work	28.2	22.6	27.5
Goto et al. (1)	18.6	34.8	27.8				
Goto et al. (2)	32.5	44.6	42.4				
Newell and Shah	31.6	32	37.7				
This work	21.7	33.7	29.7				

R507A, R125, R32). For the NIST heat transfer coefficient data, an 8.92 mm ID tube with four refrigerants (R32, R125, R134a, R410A) was used. Table 4 shows the comparison between NIST data and the proposed correlations. The Goto et al. (1) [8] and the Kedzierski and Goncalves [4] correlations showed the best prediction for the frictional pressure drops and the condensation heat transfer coefficients, respectively. The Goto et al. (1) [8] correlation showed relatively poor predicting performance for 4 and 5.1 mm ID tubes with R410A. The Kedzierski and Goncalves [4] correlation also showed poor performance for 4 mm ID tube with R410A. Table 4 shows these results.

4. Conclusions

Condensation heat transfer and pressure drop were experimentally investigated in 8.92, 6.46, 5.1, and 4 mm maximum inside diameter microfin tubes with R134a, R22, and R410A. The Kosky and Staub [21] and the Jaster and Kosky [22] heat transfer correlations and the Müller-Steinhagen and Heck [24] pressure drop correlation for smooth tubes were used to evaluate the heat transfer enhancement factors and the pressure drop penalty factors of the tested microfin tubes. The variation of the heat transfer enhancement factors with vapor quality and mass flux showed similar tendencies as those of the pressure drop penalty factors. Based on experimental data, correlations for condensation heat transfer coefficients and frictional pressure drops for the four tested microfin tubes were proposed with the heat–momentum relation.

Acknowledgements

The authors would like to express gratitude for Dr. Mark A. Kedzierski at NIST for providing the valuable experimental data and constructive suggestions and information. Furthermore, the author extends appreciation to D. Yashar for consultations on the void fraction. This work was supported by the Post-doctoral Fellowship Program of Korea Science and Engineering Foundation (KOSEF).

References

[1] K. Fujie, N. Itoh, H. Kimura, N. Nakayama, T. Yanugidi, Heat transfer pipe, US Patent 4044797, assigned to Hitachi Ltd., 1977

[2] H. Haraguchi, S. Koyama, J. Esaki, T. Fujii, Condensation heat transfer of refrigerants HCFC134a, HCFC123 and HCFC22 in a horizontal smooth tube and a horizontal microfin tube, in: Proceedings of the 30th National Symposium of Japan, Yokohama, 1993, pp. 343–345

[3] S. Nozu, H. Honda, Condensation of refrigerants in horizontal, spirally grooved microfin tubes: Numerical analysis of heat transfer in the annular flow regime, J. Heat Transfer 122 (2000) 80–91.

[4] M.A. Kedzierski, J.M. Gonclaves, Horizontal convective condensation of alternative refrigerants within a micro-fin tube, J. Enhanced Heat Transfer 6 (1999) 161–178.

[5] T.A. Newell, R.K. Shah, Refrigerant heat transfer, pressure drop, and void fraction effects in microfin tubes, in: Proceedings of the 2nd International Symposium on Two-Phase Flow and Experimentation, vol. 3, 1999, pp. 1623–1639

[6] A. Cavallini, D. Del Col, L. Doretti, G.A. Longo, L. Rossetto, Heat transfer and pressure drop during condensation of refrigerants inside horizontal enhanced tubes, Int. J. Refrig. 23 (2000) 4–25.

[7] J.Y. Choi, M.A. Kedzierski, P.A. Domanski, Generalized pressure drop correlation for evaporation and condensation in smooth and microfin tubes, in: Proceedings of IIF-IIR Commision B1, Paderborn, Germany, vol. B4, 2001, p. 9-1

[8] M. Goto, N. Inoue, N. Ishiwatari, Condensation and evaporation heat transfer of R410A inside internally grooved horizontal tubes, Int. J. Refrig. 24 (2001) 628–638.

[9] J. Yu, S. Koyama, Condensation heat transfer of pure refrigerants in microfin tubes, in: Proceedings of the International Refrigeration Conference at Purdue, 1998, pp. 325–330

[10] N. Shikazono, M. Itoh, M. Uchida, T. Fukushima, T. Hatada, Predictive equation proposal for condensation heat transfer coefficient of pure refrigerants in horizontal microfin tubes, Trans. JSME 64 (1998) 196–203.

[11] T.A. Newell, R.K. Shah, An assessment of refrigerant heat transfer, pressure drop, and void fraction effects in microfin tubes, Int. J. HVA&R Res. 7 (2) (2001) 125–153.

[12] O. García-Valladares, Review of in-tube condensation heat transfer correlations for smooth and microfin tubes, Heat Transfer Eng. 24 (4) (2003) 6–24.

[13] H.S. Wang, H. Honda, Condensation of refrigerants in horizontal microfin tubes: Comparison of prediction methods for heat transfer, Int. J. Refrig. 26 (2003) 452–460.

[14] H.S. Wang, J.W. Rose, H. Honda, Condensation of refrigerants in horizontal microfin tubes: Comparison of correlations for frictional pressure drop, Int. J. Refrig. 26 (2003) 461–472.

[15] I.E. Idelchik, Handbook of Hydraulic Resistance, third ed., CRC Press, Florida, 1994 (Chapters 3 and 4).

[16] D.A. Yashar, Experiments investigation of void fraction during horizontal flow in smaller diameter refrigeration applications, MS thesis, University of Illinois, USA, 1998

[17] ASME International, Policy on reporting uncertainties in experimental measurements and results, J. Heat Transfer 122 (2000) 411–413

[18] G. Censi, L. Doretti, L. Rossetto, C. Zilio, Flow pattern visualization during condensation of R134a inside horizontal microfin and smooth tubes, in: Proceedings of the International Congress of Refrigeration, Washington, DC, USA, 2003

[19] S. Oh, A. Bergles, Visualization of the effects of spiral angle on the enhancement of in-tube flow boiling in microfin tubes, ASHRAE Trans. 108 (Part 2) (2002) 509–515.

[20] A. Cavallini, G. Censi, D. Del Col, L. Doretti, G.A. Longo, L. Rossetto, Experimental investigation on condensation heat transfer and pressure drop of new HFC refrigerants (R134a, R125, R32, R410A, R236ea) in a horizontal smooth tube, Int. J. Refrig. 24 (2001) 73–87.
[21] P.G. Kosky, F.W. Staub, Local condensing heat transfer coefficients in the annular flow regime, AIChE J. 17 (1971).
[22] H. Jaster, P.G. Kosky, Condensation heat transfer in a mixed flow regime, Int. J. Heat Mass Transfer 19 (1976) 95–99.
[23] M.B. Ould Didi, N. Kattan, J.R. Thome, Prediction of two-phase pressure gradients of refrigerants in horizontal tubes, Int. J. Refrig. 25 (2002) 935–947.
[24] H. Müller-Steinhagen, K. Heck, A simple friction pressure drop correlation for two-phase flow in pipes, Chem. Eng. Process 20 (1986) 297–308.
[25] S.J. Eckels, B.A. Tesene, A comparison of R-22, R-134a, R-410a, and R-407c condensation performance in smooth and enhanced tubes: Part II, Pressure drop, ASHRAE Trans. 105 (1999) 428–441.
[26] A. Cavallini, C. Bortoluzzi, D. Del Col, Heat transfer enhancement and pressure gradient increase during condensation in a microfin tube: A new approach, in: Proceedings of International Congress of Refrigeration, Washington, DC, USA, 2003
[27] S.J. Eckels, B.A. Tesene, A comparison of R-22, R-134a, R-410a, and R-407c condensation performance in smooth and enhanced tubes: Part I, Heat Transfer, ASHRAE Trans. 105 (1999) 442–452.
[28] A. Cavallini, G. Censi, D. Del Col, L. Doretti, L. Rossetto, Heat transfer coefficients of HFC refrigerants during condensation at high temperature inside an enhanced tube, in: Proceedings of International Congress of Refrigeration, Washington, DC, USA, 2003
[29] D. Jung, Y. Cho, K. Park, Flow condensation heat transfer coefficients of R22, R134a, R407C, and R410A inside plain and microfin tubes, Int. J. Refrig. 27 (2004) 25–32.
[30] C.C. Wang, C.B. Chiou, D.C. Lu, Single-phase heat transfer and flow friction correlation for microfin tubes, Int. J. Heat Fluid Flow 17 (5) (1996) 500–508.
[31] J. Choi, M.A. Kedzierski, P.A. Domanski, A generalized pressure drop correlation for evaporation and condensation of alternative refrigerants in smooth and micro-fin tubes, NISTIR 6333, National Institute of Standards and Technology, Gaithersburg, Maryland, October 1999.
[32] M.A. Kedzierski, J.M. Goncalves, Horizontal convective condensation of alternative refrigerants within a micro-fin tube, NISTIR 6095, National Institute of Standards and Technology, Gaithersburg, Maryland, December 1997.